Research Article

Improving the proton conductivity of graphene oxide membranes by intercalating cations

Nur Laila Hamidah[1,2] · Masataka Shintani[1] · Aynul Sakinah Ahmad Fauzi[1] · Elaine G. Mission[1] · Kazuto Hatakeyama[3] · Armando T. Quitain[4] · Tetsuya Kida[5]

Abstract
Graphene oxide (GO) membrane has gained increasing attention because of its extraordinary physical and chemical properties and high proton conductivity. GO is rich in oxygenated functional groups, which can support proton transportation. However, pristine GO is unstable at high temperatures due to the removal of oxygen functional groups, resulting in a decrease in the interlayer distance of stacked GO nanosheets. Hence, we propose a modification of GO membranes via the intercalation of cations to enhance the proton conductivity. Modified self-standing GO membranes with Al^{3+} and La^{3+} were fabricated by a vacuum filtration method. They exhibited a larger distance of the interlayer that serves as proton hopping pathways. Furthermore, the modified GO membrane showed a higher proton conductivity than a pristine GO membrane even at 80 °C, as confirmed by Electrochemical Impedance Spectroscopy. The results demonstrate that intercalating cations in between GO nanosheets is effective in improving the practical feasibility of proton conducting GO membranes.

Keywords Graphene oxide membranes · Cations · Proton conductivity · Thermal stability

1 Introduction

Graphene oxide (GO) is a 2D material characterized with the honeycomb molecular structure. GO has gained increasing attention because of its remarkable physical, chemical and electronic properties [1]. GO contains various oxygenated functional groups such as hydroxyl, epoxy, carbonyl, and carboxyl groups. It has found potential applications in super-capacitors [2–4], catalysts [5–7], and proton conducting membranes in fuel cell or water electrolysis [8–11]. It was recently demonstrated that GO shows good proton conductivities that are comparable to that of Nafion. Epoxide groups on GO surface is considered to mainly serve as proton hopping sites [8, 12, 13].

However, GO has a tendency to lose surface functionalities even at slightly elevated temperatures. As the oxygenated functionalities detach from the carbon backbone, the interlayer distance in between stacked GO nanosheets decreases, leading to a decrease in proton conduction. Thus, maintaining the proton conductivity of GO at high temperatures is quite a challenge. In order to address this concern, GO membranes could be

Electronic supplementary material The online version of this article (https://doi.org/10.1007/s42452-019-0641-y) contains supplementary material, which is available to authorized users.

✉ Nur Laila Hamidah, nurlaila.hamidah88@gmail.com; ✉ Tetsuya Kida, tetsuya@kumamoto-u.ac.jp | [1]Department of Applied Chemistry and Biochemistry, Graduate School of Science and Technology, Kumamoto University, Kumamoto 860-8555, Japan. [2]Department of Engineering Physics, Institut Teknologi Sepuluh Nopember, Surabaya 60111, Indonesia. [3]Nanomaterials Research Institute, Department of Materials and Chemistry, National Institute of Advanced Industrial Science and Technology (AIST), Tsukuba 305-8565, Japan. [4]College of Cross-Cultural and Multi Discipline Studies, Kumamoto University, Kumamoto 860-8555, Japan. [5]Division of Materials Science, Faculty of Advanced Science and Technology, Kumamoto University, Kumamoto 860-8555, Japan.

SN Applied Sciences (2019) 1:630 | https://doi.org/10.1007/s42452-019-0641-y

Received: 25 November 2018 / Accepted: 19 May 2019 / Published online: 24 May 2019

modified through the introduction of cations. Several cations, such as Na^+, Mg^{2+}, Ca^{2+} and Al^{3+} have already been successfully applied in modifying GO in order to enhance the membrane stability in aqueous solution for desalination and separation applications [14–17]. These cations would form ionic interaction with the negatively charged GO nanosheets. Amirov et al. [18, 19] reported that carboxyl groups in GO behave as ligands, which bind to metal cations via chemical bonding.

This study focused on the intercalation of the lanthanum cation (La^{3+}) in between stacked GO nanosheets. La^{3+}-based materials have been considered as an attractive material for electrochemical-based systems [20–22]. We studied the effect of La^{3+} and Al^{3+} intercalation on the proton conductivity of GO membranes by an EIS technique and examined the correlation between proton conductivity and physicochemical properties.

2 Experimental section

2.1 Synthesis of GO and membrane fabrication

GO was prepared from synthetic graphite powder (Wako Pure Chemical Industries, Osaka, Japan) following the modified Hummers' method. The detailed procedure has already been reported elsewhere [23, 24]. Briefly, graphite was first oxidized into graphite oxide with sulfuric acid and potassium permanganate. The oxidized graphite was cooled and recovered from liquid by centrifugation at 4000 rpm for 30 min. The precipitates were then washed with a HCl aqueous solution (5%) by centrifugation at 4000 rpm for 30 min three times to remove K^+ and Mn^+. The solid products were washed with distilled water by centrifugation at 4000 rpm for 30 min three times. Graphite oxide was ultrasonicated for 5 h to obtain GO nanosheets, which were redispersed in distilled water to make a GO dispersion. Subsequently, 0.01 mmol of aluminum nitrate [$Al(NO_3)_3$, > 98.0%, Chameleon reagent under Kishida Kagaku, Japan) and lanthanum nitrate [$La(NO_3)_3$, Wako Pure Chemical Industries, Osaka, Japan] were separately added into the GO dispersion. The mixed solution of GO and cation was poured onto membrane filters (180 µm and 0.4 µm membrane filter stacked together). Then, the system was subjected to vacuum filtration at room temperature and atmospheric pressure. A self-standing membrane formed was separated from the supporting membrane filters. The final concentration of the intercalated cations was estimated through the mass differences between pristine GO and modified GO membranes. The thickness of the membranes was 180 µm.

2.2 Materials characterization

The structure and interlayer spacing in between GO nanosheets of the fabricated GO membrane were characterized by X-ray diffraction (XRD; MiniFlex600, Rigaku) with Cu Kα radiation (λ = 0.154 nm, U = 40 kV and I = 15 mA) in the 2θ range of 5°–45°. The morphology of GO nanosheets was observed by scanning electron microscopy (SEM; JSM7600F, JEOL) and atomic force microscopy (AFM). The size distribution of the GO nanosheets was examined with a DLS spectrophotometer (Zetasizer Nano ZS, Malvern Instruments). The presence of oxygen functional groups was analyzed using a Fourier transform infrared (FT-IR) spectrometer (FTIR 4100, JASCO) through the KBr pellet technique and X-ray photoemission spectroscopy (XPS; PHI 1600, PerkinElmer). Thermal stability of samples were examined by thermogravimetric-differential thermal analysis (TG–DTA; SII Exstar 6000, SEIKO) at 25 to 300 °C with the heating rate of 10 °C/min under a constant nitrogen flow (20 mL/min). The BET surface area was measured with a surface area analyzer (BELSORP-mini II, Microtrack Bell) under nitrogen atmosphere at 77 K. For the pretreatment, samples were heated under N_2 at 60 °C for 24 h.

2.3 Proton and electrical conductivity measurement

The proton conductivities of GO and modified GO membranes were measured by AC impedance spectroscopy using an impedance analyzer (1260, Solartron) over the frequency range of 1 Hz to 1 MHz with the test signal voltage of 100 mV. Platinum (Pt) was deposited onto the membrane surface as the electrodes using a sputtering technique. The membrane was placed in an incubator, and its impedance was measured at 25 to 80 °C. The electrical conductivity of the membrane was also measured by a two-probe DC method using a multimeter (33410A, Agilent).

The proton and electrical conductivities were calculated following Eq. 1,

$$\sigma = \frac{l}{A \cdot Rs} \tag{1}$$

where σ (S cm^{-1}) is the conductivity of the membranes, l (cm) is the membrane thickness, and A (cm) and Rs (Ω) represent the cross section area and the resistances of the membranes measured by AC impedance spectroscopy as well as by a two probe DC method, respectively. A Nyquist plot was obtained using impedance values fitted based on the proposed equivalent circuit as depicted in Fig. 1,

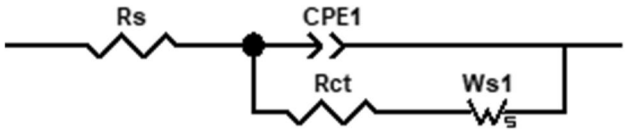

Fig. 1 Equivalent circuit of GO membranes

where Rs is the bulk resistance and CPE is the constant phase element employed to replace the capacitance (C) element to get the fitting result more precisely, while Rct and Ws1 represent the charge transfer resistance and the Warburg impedance associated with ionic diffusion of the membrane [25–27], respectively.

3 Result and discussion

3.1 GO membrane characterization

The exfoliation of GO nanosheets was confirmed by SEM, DLS, and AFM analyses, as shown in Fig. S1 (supplementary materials). A representative SEM image shows a sheet-like structure of the sample. The thickness of GO nanosheets was estimated to be 1.1 nm by the AFM results. The presence of smaller GO nanosheets of 200 to 300 nm was mainly seen by DLS analysis. The surface area of GO was calculated to be 35 m^2/g from the nitrogen adsorption/desorption isotherm (Fig. S2), which was the type IV isotherm typically for mesoporous materials. The low N_2 adsorption and low pore volumes indicate the intimate stacking of GO nanosheets. Figure 2 shows the XRD patterns of membranes made of pristine GO in comparison with those with Al^{3+} and La^{3+}. All three XRD patterns showed a single sharp peak. The characteristic peak for the pristine GO membrane was observed at $2\theta = 9.4°$, indicating the introduction of oxygen functional groups onto graphene sheets [28].The XRD peaks for Al^{3+} and La^{3+}-modified GO membranes slightly shifted to a lower degree of $2\theta = 8.8°$ and 7.9°, respectively. The shift could be an indication of the alteration in the crystallinity and interlayer structure of the GO membranes due to the presence of ionic interaction between oxygen functional groups and the cations. The interlayer spacing (d) was also found to change. The pristine GO membrane has d = 9.4 Å while Al^{3+} and La^{3+}-modified GO membranes have d = 10.3 and 10.8 Å, respectively. Clearly, the intercalation of cations increased the interlayer spacing. The slight difference in d-spacing for Al^{3+} and La^{3+} could be attributed to the difference between their atomic radii. La^{3+} has a bigger atomic radius of 2.7 Å than Al^{3+} with an atomic radius of 1.4 Å.

FTIR spectra of pristine GO and Al^{3+} and La^{3+}-modified GO membranes are shown in Fig. 3. The broad peak between 3200 and 3700 cm^{-1} is regularly attributed to the presence of hydroxyl groups. It can be seen that there is no significant difference in hydroxyl functionalities for the three samples. The C=O stretching vibration at 1725 cm^{-1} was maintained. However, for the Al^{3+} and La^{3+}-modified GO membranes, a small peak at 1480 cm^{-1} was observed. This was previously ascribed to the formation of carboxylate chelates, for which carboxyl groups in GO should bind to Al^{3+} and La^{3+} [14]. The presence of oxygen functional groups was also confirmed by XPS analysis, as shown in Fig. S3. The oxygen content in GO was determined to be 57 wt%.

We also estimated the amount of intercalated cations. On average, Al^{3+} amounted to 1.3 ± 0.3 mg, i.e., about

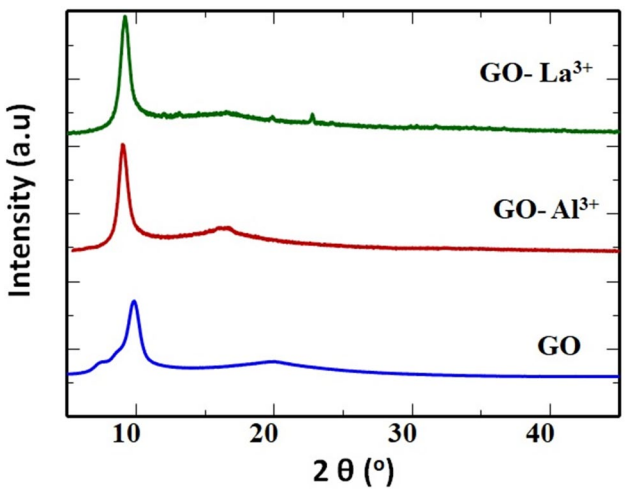

Fig. 2 XRD patterns of pristine GO and cation modified GO membranes

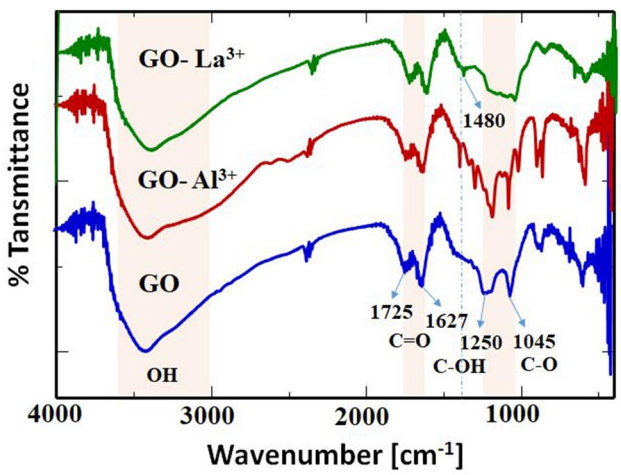

Fig. 3 FTIR spectra of pristine GO membrane and cation modified GO membranes

8 wt% of the modified GO membrane. On the other hand, there was about 2.7 ± 0.3 mg of La^{3+} recorded, corresponding to 16 wt% of the modified GO membrane. The amount of La^{3+} contained is higher than that of Al^{3+}. This might be due to the higher solubility of lanthanum nitrate in water (123–158 g per 100 ml) compared to that of aluminum nitrate with the solubility of 73.9 g per 100 ml. The higher amount of La^{3+} intercalated would contribute to the observed increase in the interlayer distance, as suggested by the XRD results.

3.2 Electrochemical impedance spectroscopy (EIS)

Electrochemical impedance spectroscopy (EIS) is the most reliable and effective technique to obtain the electrochemical characteristics of an electrochemical system [29]. We used an EIS technique to study the proton conduction in the GO membranes. EIS data were used to draw Nyquist plots that are represented in complex impedance plane consisting of real impedance (Z′) in X-axis and imaginary impedance (Z″) in Y-axis. From the equivalent circuit depicted in Fig. 1, we expect that the Nyquist plots become a depressed semicircle representing the internal impedance of the GO membrane. Fig. 4 shows the Nyquist plots of the pristine GO membrane in comparison with those for Al^{3+} and La^{3+}-modified GO membranes at varying temperatures. Depressed semicircles were generated for all the membranes. At the high frequency region (Fig. 4a inset), (1) the intersection between X-axis and the starting point of the curve represents the sum of the membrane bulk resistance (Rs) and the contact resistance between the Pt electrode and a Pt mesh as a current collector and (2) the radius of the semicircles represents the charge transfer resistance of the electrode material [30]. The pristine GO membrane (Fig. 4a) showed a distinct semicircle at high frequency that corresponded to the double layer capacitance of the Pt electrode-membrane interface and the charge transfer resistance (Rct) [31]. A distinct capacitive semicircle was also generated for the Al^{3+}-modified GO membrane. On the other hand, the membrane with La^{3+} showed a half capacitive semicircle that corresponded to a low charge transfer resistance.

The bulk resistance of the membranes increased as temperature increased. The pristine GO (Fig. 4a) membrane showed a bulk resistance (Rs) at around 1.5 kΩ. However, at 80 °C, the Rs increased significantly and reached 9.1 kΩ. When Al^{3+} was intercalated in between GO nanosheets, the Rs was lowered to 1.4 kΩ (Fig. 4b). The Rs was stable until 60 °C, but then it significantly increased at 80 °C. For the La^{3+}-modified GO membrane (Fig. 4c), the maximum Rs was below 1 kΩ. The Rs was almost stable even up to 80 °C. The resistance at high temperatures was almost

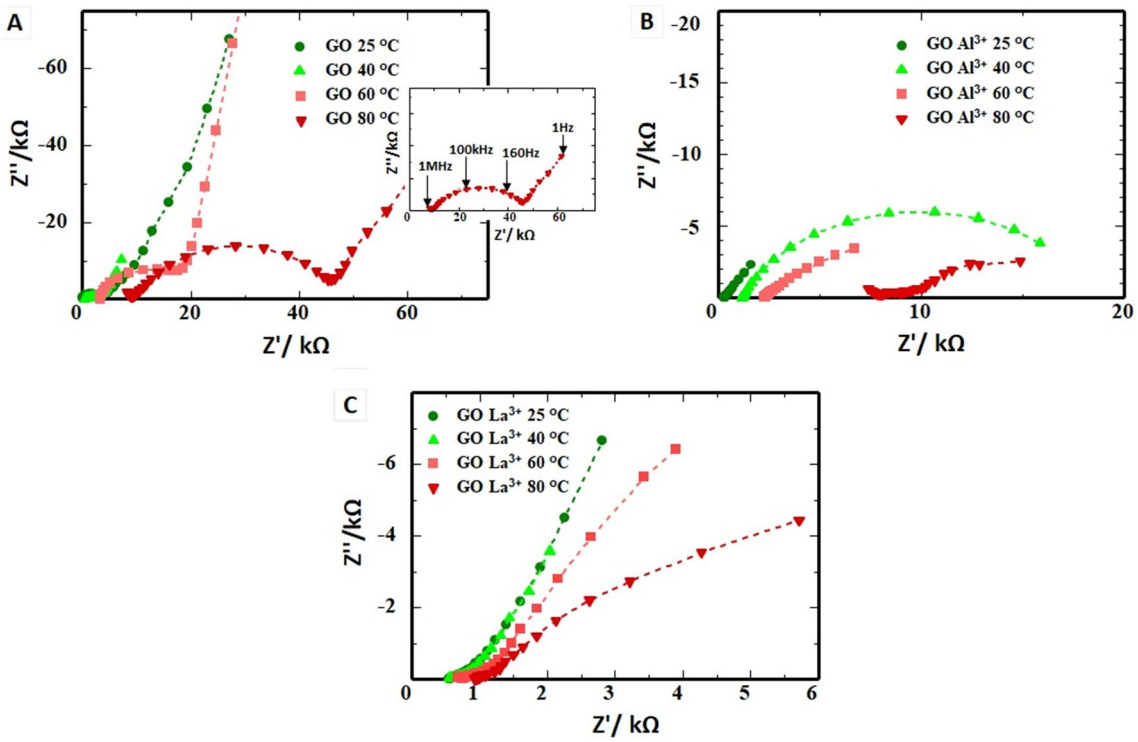

Fig. 4 Nyquist plots of GO membranes at different temperatures. **a** Pristine GO membrane, **b** modified GO membrane with 0.01 mmol of Al^{3+} and **c** modified GO membrane with 0.01 mmol of La^{3}

constant for the La^{3+}-modified GO membrane, indicating its lower charge transfer resistance and bulk resistance even at high temperatures. At low frequency region, the slope of 45° in Nyquist plots is denoted as the Warburg resistance that represents the ionic diffusion/transport in the membrane. The membrane with La^{3+} showed a 45° slope at lower temperature, suggesting good ionic diffusion in GO [30]. In contrast, the 45° slope at low frequency region was absent for the membrane with Al^{3+}.

3.3 Proton and electrical conductivity

In Fig. 5, the temperature dependences of proton conductivity of the pristine, Al^{3+}, and La^{3+}-modified GO membranes are summarized. Pristine GO showed the lowest proton conductivity and its proton-conducting ability was found to decrease as temperature increased. The pristine GO membrane losses oxygenated functional groups, leading to the loss of proton conduction, particularly at higher than 60 °C.

The loss in oxygen functional groups was confirmed by TG–DTA analysis, as depicted in Fig. 6, which showed that decreases in weight by 10 and 20% were noted at R.T. to 60 and 60 to 140 °C, respectively. These losses were attributed to the removal of oxygen functional groups on GO. The complete combustion of pristine GO occurred at 150 °C. On the contrary, both the Al^{3+} and La^{3+}-modified GO membranes demonstrated much better proton conductivity than the pristine GO membrane. This demonstrates that the intercalation of cations indeed contributed to the improvement in proton conductivity. However, Al^{3+} still suffered a decline in proton conducting activity as temperature increased. On the other hand, the La^{3+}-modified membrane maintained the superior proton conductivity compared with other membranes tested. One possible explanation is the enhanced hydration of the membrane with La^{3+} due to the larger interlayer spacing and the resulting efficient proton hopping in the interlayer. In addition, La^{3+} improved the stability of the membrane probably due to formation of cross links between GO nanosheets. An improvement in the thermal stability was confirmed by the TG–DTA results (Fig. 6). The TG curves showed that the weight loss due to removal of oxygen functional groups was suppressed by introducing Al^{3+} and La^{3+} in the interlayer. In addition, the presence of cations even suppressed the combustion of GO. A DTA peak due to the combustion of GO shifted from 140 to 175 °C and 200 °C by Al^{3+} and La^{3+} cation introduction, respectively. The TG results indicate that the intercalated amounts of Al^{3+} and La^{3+} were 12 and 23%, respectively. Intercalating La^{3+} with the larger amount in a GO membrane likely improved the thermal stability, leading to the higher proton conductivity.

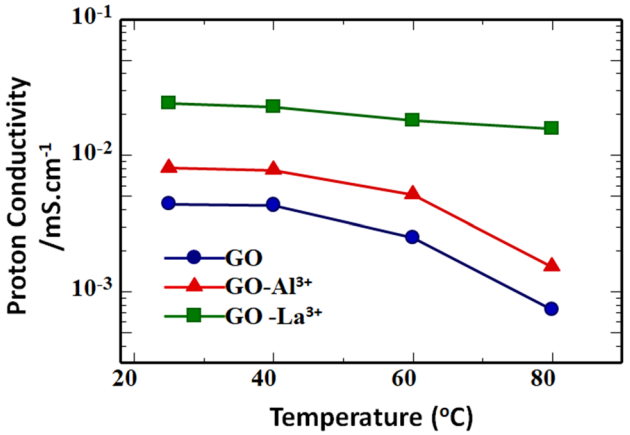

Fig. 5 Dependence of proton conductivity on temperature for the pristine and modified GO membranes. The relative humidity was 70%

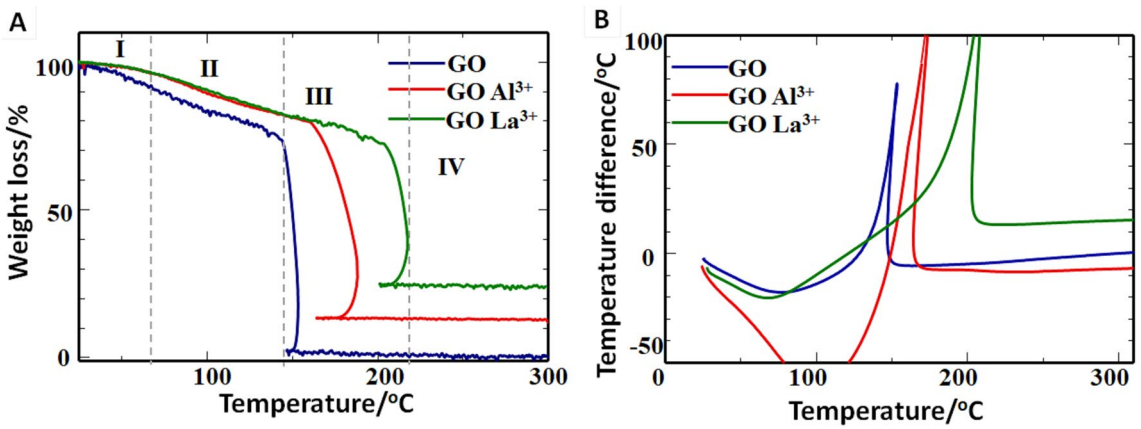

Fig. 6 **a** Thermogravimetric analysis (TGA) and **b** differential thermal analysis (DTA) curves of GO nanosheets in nitrogen atmosphere

We also measured the electrical conductivity of the membranes. Figure 7 shows the temperature dependence of electrical conductivity of the pristine and modified GO membranes. At 25 and 40 °C, the electrical conductivity of all the membranes was low in the range of $R = 0.5 \times 10^{-7}$ to 10^{-8} S/cm, making them pure solid electrolytes. However, the electrical conductivity of the membranes with cations significantly increased at more than 60 °C, while that for the pristine GO membrane remained low. The increase in the electrical conductivity can be explained by partial detachment of oxygen functional groups and the resulting increase in sp2-carbon regions in the membranes [32]. However, the detailed mechanism is not clear yet. Nevertheless, increasing the electrical conductivity while maintaining the high proton conductivity is favorable in terms of mixed proton-electron conduction, which would enable novel applications of GO such as electrocatalysts [12, 32].

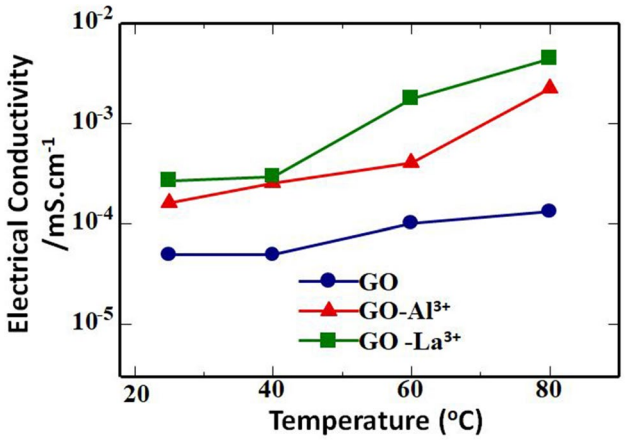

Fig. 7 Dependence of electrical conductivity on temperature for the pristine and modified GO membranes. The relative humidity was 70%

3.4 Post-treatment characterization of GO membranes

The GO membranes after thermal treatment (80 °C) were characterized to clarify the correlation between conductivity and physicochemical properties of GO. The XRD and FTIR profiles collected are shown in Fig. 8a. The XRD peaks broadened and slightly shifted to the right. For instance, in the case of pristine GO, it shifted from $2\theta = 9.4°$ to 10.5°, corresponding to a decrease in d-spacing. This is a typical characteristic of GO when it loses some oxygenated functionalities from its surface. The d-spacings are summarized in Table 1. After heat treatment, for pristine GO the d-spacing decreased by as much as 20%, while for GO-Al^{3+} it decreased by 18%. Interestingly, GO-La^{3+} only exhibited a 9% decrease in d-spacing. It is thus concluded that the smallest change in d-spacing allowed the membrane with La^{3+} to maintain its stable proton conductivity even at high temperatures.

Changes in chemical structure of GO after thermal treatment (80 °C) were also examined by FTIR measurements, as depicted in Fig. 8b. After thermal treatment, the absorption peak at 3400 cm^{-1} that corresponded to O–H group greatly decreased for pristine GO as well as GO with Al^{3+}. In contrast, for GO with La^{3+} only a slight decrease was

Table 1 The interlayer distance of the pristine GO and modified GO membranes after heat treatment at 80 °C

Cation types	Room temperature		After high temperature treatment	
	2θ (°)	d spacing (Å)	2θ (°)	d spacing (Å)
GO	9.4	9.4	10.5	7.5
GO-Al^{3+}	8.8	10.3	9.9	8.4
GO-La^{3+}	7.9	10.8	9.1	9.9

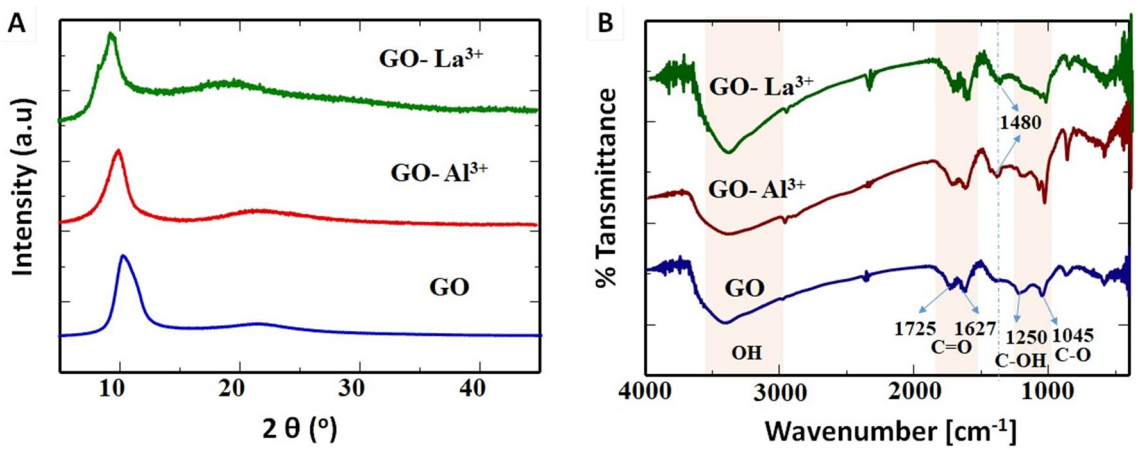

Fig. 8 **a** XRD patterns and **b** FTIR spectra of the pristine GO and modified GO membranes after heat treatment at 80 °C

observed. Furthermore, a decrease in absorption peak at 1725 and 1627 cm^{-1} ascribable to C=O was seen for pristine GO and GO with Al^{3+}. However, almost no change in C=O peak was seen for GO with La^{3+}. The FTIR results indicate that GO with La^{3+} maintained oxygen functional groups even after thermal treatment. The strong interaction of La^{3+} with oxygen functional groups may retard their desorption from GO, allowing protons diffuse on GO nanosheets even at higher temperature.

4 Conclusion

We have successfully fabricated cation-modified GO membranes by introducing Al^{3+} and La^{3+} in a GO suspension prior to the membrane fabrication. The intercalated cations, especially La^{3+}, can significantly increase the proton conductivity of the membrane, possibly due to the ionic interaction between oxygen functional groups and the cations. This resulted in an increase in distance of the interlayer that functioned as a proton hopping pathway. The presence of La^{3+} in GO membranes prevented detachment of oxygen functional groups at high temperatures, as suggested by XRD, FTIR, TG–DTA, and EIS results. Accordingly, the proton conductivity was maintained even at high temperature. The findings obtained here would expand the possibility of electrochemical applications of proton-conducting GO membranes and also provide ever better performance.

Acknowledgements We thank Prof. Mitsuru Sasaki for his assistance to perform TG–DTA measurements.

Funding This work was supported in part by the JST e-ASIA collaborative research Project on functional materials, a Grant-in-Aid for the Promotion of Joint International Research (15KK0189), and a Grant-in-Aid for Scientific Research (B) (18H01835) from the Ministry of Education, Culture, Sports, Science and Technology of Japan. T. K. also acknowledges the support from Kato foundation for Promotion of Science, Japan (KJ-2822).

Compliance with ethical standards

Conflict of interest On behalf of all authors, the corresponding author states that there is no conflict of interest.

Ethical approval This article does not contain any studies involving animals performed by any of the authors.

References

1. Dimiev AM (2016) Mechanism of formation and chemical structure of graphene oxide. In: Dimiev AM, Eigler S (eds) Graphene oxide. Wiley, Hoboken, pp 36–84
2. Ogata C, Kurogi R, Awaya K, Hatakeyama K, Taniguchi T, Koinuma M, Matsumoto Y (2017) All-graphene oxide flexible solid-state supercapacitors with enhanced electrochemical performance. ACS Appl Mater Interfaces 9:26151–26160. https://doi.org/10.1021/acsami.7b04180
3. Down MP, Rowley-Neale SJ, Smith GC, Banks CE (2018) Fabrication of graphene oxide supercapacitor devices. ACS Appl Energy Mater 1:707–714. https://doi.org/10.1021/acsaem.7b00164
4. Purkait T, Singh G, Kumar D, Singh M, Dey RS (2018) High-performance flexible supercapacitors based on electrochemically tailored three-dimensional reduced graphene oxide networks. Sci Rep. https://doi.org/10.1038/s41598-017-18593-3
5. Behling R, Valange S, Chatel G (2016) Heterogeneous catalytic oxidation for lignin valorization into valuable chemicals: what results? What limitations? What trends? Green Chem 18:1839–1854. https://doi.org/10.1039/C5GC03061G
6. Grigoriev S, Fateev V, Pushkarev A, Pushkareva I, Ivanova N, Kalinichenko V, Presnyakov MY, Wei X (2018) Reduced graphene oxide and its modifications as catalyst supports and catalyst layer modifiers for PEMFC. Materials 11:1405. https://doi.org/10.3390/ma11081405
7. Majumdar B, Sarma D, Bhattacharya T, Sarma TK (2017) Graphene oxide as metal-free catalyst in oxidative dehydrogenative C–N coupling leading to α-ketoamides: importance of dual catalytic activity. ACS Sustain Chem Eng 5:9286–9294. https://doi.org/10.1021/acssuschemeng.7b02267
8. Kida T, Kuwaki Y, Miyamoto A, Hamidah NL, Hatakeyama K, Quitain AT, Sasaki M, Urakawa A (2018) Water vapor electrolysis with proton-conducting graphene oxide nanosheets. ACS Sustain Chem Eng 6:11753–11758. https://doi.org/10.1021/acssuschemeng.8b01998
9. Thimmappa R, Chattanahalli Devendrachari M, Shafi S, Freunberger S, Ottakam Thotiyl M (2016) Proton conducting hollow graphene oxide cylinder as molecular fuel barrier for tubular H 2-air fuel cell. Int J Hydrogen Energy 41:22305–22315. https://doi.org/10.1016/j.ijhydene.2016.08.057
10. Tateishi H, Hatakeyama K, Ogata C, Gezuhara K, Kuroda J, Funatsu A, Koinuma M, Taniguchi T, Hayami S, Matsumoto Y (2013) Graphene oxide fuel cell. J Electrochem Soc 160:F1175–F1178. https://doi.org/10.1149/2.008311jes
11. Jang HR, Vinothkannan M, Kim AR, Yoo DJ (2018) Constructing proton-conducting channels within sulfonated(poly arylene ether ketone) using sulfonated graphene oxide: a nano-hybrid membrane for proton exchange membrane fuel cells: constructing proton-conducting channels within sulfonated (poly arylene ether ketone). Bull Korean Chem Soc 39:715–721. https://doi.org/10.1002/bkcs.11459
12. Hatakeyama K, Islam MS, Michio K, Ogata C, Taniguchi T, Funatsu A, Kida T, Hayami S, Matsumoto Y (2015) Super proton/electron mixed conduction in graphene oxide hybrids by intercalating sulfate ions. J Mater Chem A 3:20892–20895. https://doi.org/10.1039/C5TA05653E
13. Hatakeyama K, Karim MR, Ogata C, Tateishi H, Funatsu A, Taniguchi T, Koinuma M, Hayami S, Matsumoto Y (2014) Proton conductivities of graphene oxide nanosheets: single, multilayer, and modified nanosheets. Angew Chem Int Ed 53:6997–7000. https://doi.org/10.1002/anie.201309931
14. Wenzheng Y, Yu T, Graham N (2017) Development of a stable cation modified graphene oxide membrane for water treatment. 2D Mater 4:045006
15. Mo Y, Zhao X, Shen Y (2016) Cation-dependent structural instability of graphene oxide membranes and its effect on membrane separation performance. Desalination 399:40–46. https://doi.org/10.1016/j.desal.2016.08.012
16. Xu X-L, Lin F-W, Du Y, Zhang X, Wu J, Xu Z-K (2016) Graphene oxide nanofiltration membranes stabilized by cationic porphyrin for high salt rejection. ACS Appl Mater Interfaces 8:12588–12593. https://doi.org/10.1021/acsami.6b03693

17. Huang H, Song Z, Wei N, Shi L, Mao Y, Ying Y, Sun L, Xu Z, Peng X (2013) Ultrafast viscous water flow through nanostrand-channelled graphene oxide membranes. Nat Commun 4:2979
18. Amirov RR, Shayimova J, Nasirova Z, Dimiev AM (2017) Chemistry of graphene oxide. Reactions with transition metal cations. Carbon 116:356–365. https://doi.org/10.1016/j.carbon.2017.01.095
19. Amirov RR, Shayimova J, Nasirova Z, Solodov A, Dimiev AM (2018) Analysis of competitive binding of several metal cations by graphene oxide reveals the quantity and spatial distribution of carboxyl groups on its surface. Phys Chem Chem Phys 20:2320–2329. https://doi.org/10.1039/C7CP07055A
20. Hjalmarsson P, Søgaard M, Hagen A, Mogensen M (2008) Structural properties and electrochemical performance of strontium- and nickel-substituted lanthanum cobaltite. Solid State Ion 179:636–646. https://doi.org/10.1016/j.ssi.2008.04.026
21. Hrovat M, Bernik S, Kuscer D, Holc J, Katsarakis N, Reichmann K (1996) Characterisation of LaNi{sub 1}-xCo{sub x}O{sub 3} as a possible SOFC cathode material. Solid State Ion. https://doi.org/10.1016/0167-2738(95)00224-3
22. Chou C-Y, Kaurav N, Kuo Y-K, Kuo D-H (2008) Electrical properties of A/B-site substituted Ni-deficient $La(Ni_{0.6}Fe_{0.3})O_3$ perovskites with $A = Ag^{+}$, Pb^{2+}, Nd^{3+} and $B = Mn^{3+}$, Ga^{3+}. J Appl Phys. https://doi.org/10.1063/1.2924424
23. Miyamoto A, Kuwaki Y, Sano T, Hatakeyama K, Quitain A, Sasaki M, Kida T (2017) Solid electrolyte gas sensor based on a proton-conducting graphene oxide membrane. ACS Omega 2:2994–3001. https://doi.org/10.1021/acsomega.7b00239
24. Mission EG, Quitain AT, Sasaki M, Kida T (2017) Synergizing graphene oxide with microwave irradiation for efficient cellulose depolymerization into glucose. Green Chem 19:3831–3843. https://doi.org/10.1039/C7GC01691C
25. Chen F, Liu P (2011) Conducting polyaniline nanoparticles and their dispersion for waterborne corrosion protection coatings. ACS Appl Mater Interfaces 3:2694–2702. https://doi.org/10.1021/am200488m
26. Guo X, Du K, Wang Y, Shao Y, Wang F (2012) A new nanoparticle penetrant used for plasma electrolytic oxidation film coated on AZ31 Mg alloy in service environment. Surf Coat Technol 206:4833–4839. https://doi.org/10.1016/j.surfcoat.2012.05.063
27. Lu F, Song B, He P, Wang Z, Wang J (2017) Electrochemical impedance spectroscopy (EIS) study on the degradation of acrylic polyurethane coatings. RSC Adv 7:13742–13748. https://doi.org/10.1039/C6RA26341K
28. Johra FT, Lee J-W, Jung W-G (2014) Facile and safe graphene preparation on solution based platform. J Ind Eng Chem 20:2883–2887. https://doi.org/10.1016/j.jiec.2013.11.022
29. Ates M (2011) Review study of electrochemical impedance spectroscopy and equivalent electrical circuits of conducting polymers on carbon surfaces. Prog Org Coat 71:1–10. https://doi.org/10.1016/j.porgcoat.2010.12.011
30. Gong Y, Li D, Fu Q, Pan C (2015) Influence of graphene microstructures on electrochemical performance for supercapacitors. Prog Nat Sci Mater Int 25:379–385. https://doi.org/10.1016/j.pnsc.2015.10.004
31. Fasmin F, Srinivasan R (2017) Review—nonlinear electrochemical impedance spectroscopy. J Electrochem Soc 164:H443–H455. https://doi.org/10.1149/2.0391707jes
32. Hatakeyama K, Tateishi H, Taniguchi T, Koinuma M, Kida T, Hayami S, Yokoi H, Matsumoto Y (2014) Tunable graphene oxide proton/electron mixed conductor that functions at room temperature. Chem Mater 26:5598–5604. https://doi.org/10.1021/cm502098e